Petroleum Science 21 (2024) 2688–2702

Contents lists available at ScienceDirect

Petroleum Science

journal homepage: www.keaipublishing.com/en/journals/petroleum-science

Original Paper

Multiple damage zones around hydraulic fractures generated by high-frequency pulsating hydraulic fracturing

Yan Peng [a, *], Sheng-Jie Wei [a], Guang-Qing Zhang [a], Da-Wei Zhou [a], Chuang-Chao Xu [b]

[a] School of Petroleum Engineering, China University of Petroleum, 18 Fuxue Road, Changping, Beijing, 102249, China
[b] PetroChina Changqing Oilfield Company, Xi'an, 710018, Shaanxi, China

ARTICLE INFO

Article history:
Received 30 October 2023
Received in revised form
13 May 2024
Accepted 13 May 2024
Available online 15 May 2024

Edited by Jia-Jia Fei

Keywords:
Tight reservoir
Reservoir stimulation
Numerical simulation
Secondary fracture
Fracture initiation

ABSTRACT

Pulsating hydraulic fracturing (PHF) is a promising fracturing method and can generate a dynamic periodic pressure. The periodic pressure can induce fatigue failure of rocks and decrease initiation pressure of fracture. If the frequency of periodic pressure exceeds 10 Hz, the distribution of pressure along the main fracture will be heterogeneous, which is much different from the one induced by the common fracturing method. In this study, the impact of this special spatial feature of pressure on hydraulic fracture is mainly investigated. A coupled numerical simulation model is first proposed and verified through experimental and theoretical solutions. The mechanism of secondary fracture initiation around the main fracture is then discovered. In addition, sensitivity studies are conducted to find out the application potential of this new method. The results show that (1) this coupled numerical simulation model is accurate. Through comparison with experimental and theoretical data, the average error of this coupled model is less than 1.01%. (2) Even if a reservoir has no natural fracture, this heterogeneous distribution pressure can also cause many secondary fractures around the main fracture. (3) The mechanism of secondary fracture initiation is that this heterogeneous distribution pressure causes tensile stress at many locations along the main fracture. (4) Through adjusting the stimulation parameters, the stimulation efficiency can be improved. The average and amplitude of pressure can increase possibility of secondary fracture initiation. The frequency of this periodic pressure can increase number of secondary fractures. Even 6 secondary fractures along a 100 m-length main fracture can be generated. (5) The influence magnitudes of stimulation parameters are larger than ones of geomechanical properties, therefore, this new fracturing method has a wide application potential.

1. Introduction

Pulsating hydraulic fracturing (PHF) method can decrease initiation pressure of hydraulic fractures (Zhi et al., 2017; Zang et al., 2017b), decrease seismicity (Zang et al., 2013, 2018) and create complicated hydraulic fracture networks. It has been applied at shale reservoirs (Chang et al., 2022; Wu et al., 2023) and hot dry rock (HDR) geothermal reservoirs (Zang et al., 2021; Liu Y. et al., 2022). The PHF can be simply completed by periodically change pumping rate (Haimson and Cornet, 2003; Zang et al., 2017b; Ciezobka et al., 2018; Sullivan and Grieser, 2017; Zimmermann et al., 2019) and generate a periodic pressure. However, the frequency of periodic pressure generated by this method is usually less than 4 Hz. In this case, the mechanism of decreasing hydraulic fracture generation difficulty is mainly the rock fatigue failure (Zang et al., 2013, 2017a; Zhou et al., 2017; Zhi et al., 2017; Xu et al., 2019; Hou et al., 2022a).

The impacts of the PHF stimulation parameters on hydraulic fracture have been investigated. The PHF stimulation scheme affects hydraulic fractures. The stepwise pulse pressurization scheme can significantly decrease breakdown pressure by around 24% (Jung et al., 2021; Zhuang et al., 2019, 2020; Chang et al., 2022) and decrease seismic energy (Ji et al., 2021). The controlled-pressure uniform cyclic injection scheme can enhance permeability up to 3 times (Zang et al., 2013; Zimmermann et al., 2019; Goyal et al., 2020). These advantages of the PHF result from the rock fatigue failure so the circle number of periodic pressure is important. The fatigue lifetime (required circle number of periodic pressure to

* Corresponding author.
E-mail address: yan.peng@cup.edu.cn (Y. Peng).

https://doi.org/10.1016/j.petsci.2024.05.007

broke an intact rock) of shale rocks and granite rocks is usually several hundreds or even be up to one thousand (Diaz et al., 2018; Hou et al., 2022a). The hydraulic fracturing experiment points out that the require circle number sharply decreases. This experiment uses a rock sample with a hole in sample center and hydraulic fluid is injected through this hole. There may be microcracks generated during drilling this hole. The circle number depends on the upper limit pressure of periodic pressure. If the upper limit pressure reaches at 90% breakdown pressure of rock, the required circle number will be only 7 (Wu et al., 2023). If the upper limit pressure is 60% of breakdown pressure, the required circle number will significantly increase to be over 40 (Wu et al., 2023). In real hydraulic fracturing stimulation, the circle number of periodic pressure is usually less than 10 (Zang et al., 2017a; Sullivan and Grieser, 2017; Zimmermann et al., 2019), which is obviously less than fatigue lifetime. Therefore, the fatigue failure may be hard to be occurred in those PHF stimulations.

The PHF can induce the pressure wave propagation inside fluid-filled pipes, which is well known as the water hammer phenomenon (Su et al., 2003; He et al., 2022). The superposition effects of the pressure waves make borehole pressure different from the one of common hydraulic fracturing (Zhai et al., 2015; Xu et al., 2017, 2018; Ma et al., 2017; Wu et al., 2020). Experimental data from Zhai et al. (2015) showed that input frequency increases amplitudes of pressure waves. The experimental results indicate that pressure inside pipe initially fluctuates with time and then stays at a stable state (He et al., 2018). The numerical simulation is the other way to investigate the fluid flow behavior of the PHF. The common models include: a percolation model, an oscillation flow model, a one-dimensional pressure wave equation, and a transient flow model (TFM). The percolation model was proposed based on Darcy's law (Rehbinder, 1980) and it was only available for blocked fractures (Liu et al., 2007; Li et al., 2015). The oscillation flow model was proposed based on Poiseuille flow, and the pressure wave propagation was assumed to relate to the average velocity and acceleration of a fluid in a cross-section (Zhao and Liang, 1998). This model was only available when fractures disintegrate completely and vibrate with the pulse pressure (Li et al., 2015; Liu et al., 2007). The one-dimensional pressure wave equation was proposed by Jiang and Xing (2018) but it ignored the friction effect leading inaccuracy about pressure wave propagation features. The TFM was proposed by Fiorotto and Rinaldo (1992) and pressure wave was directly assumed as a wave and the friction effect was also considered. This model was solved by the method of characteristics (MOC). Many scholars used this method to investigate the pressure wave features in pipes and fractures (Liu, 1994; Oliveira et al., 2013; Wang et al., 2015; Zhai et al., 2015; Sławomir, 2018; Zhang et al., 2018). Its accuracy was validated by experimental data (Hou et al., 2021). Zhang et al. (2018) used the TFM to study the pressure wave propagation in coiled tubing drilling pipes and concluded that an input frequency (8, 12, 15, or 20 Hz) has almost no effect on pressure amplitude. Hou et al. (2021) used this method to investigate the pressure wave features in pipes. The main frequency of pressure wave was found out to be close to the resonance frequency of fluid inside pipes. Hou et al. (2022b) used this method to investigate the pressure wave features in fractures. The results showed that a standing wave is formed in fractures and the number of its peak values depends on input frequency. If the high-frequency periodic pressure is used (frequency is higher than 10 Hz), over 2 pressure peak values could be generated. This kind of pressure inside fracture has a potential to generate several secondary fractures around main fracture. However, its availability to generate secondary fractures and its controlling factors have not been fully investigated.

In this study, the main purpose is to investigate the mechanism of secondary fracture initiation induced by high-frequency pulsating hydraulic fracturing and to find out its controlling factors. Firstly, the numerical simulation coupling pulsating pressure wave in fractures, rock deformation and rock damage was proposed. The pulsating pressure wave equation describes the fluid flow features inside fractures. The rock deformation equation predicts the rock stress. The rock damage equation evaluates the initiations of secondary fractures around main hydraulic fracture. Secondly, those equations were then validated by experimental data and theoretical solutions. Thirdly, through this coupling numerical simulation, the mechanism of secondary fracture initiation induced by the high-frequency PHF was discovered and the controlling factors were discussed. The results can provide technical guidance to engineering applications.

2. Numerical simulation model

2.1. Conceptual model

After the main hydraulic fractures is generated, the pulsating pressure can be generated by some instruments or methods, such as the self-excited pulsed jet device (Pang et al., 2022), hydraulic pulse oscillation tools (Shi et al., 2021) and periodic injection

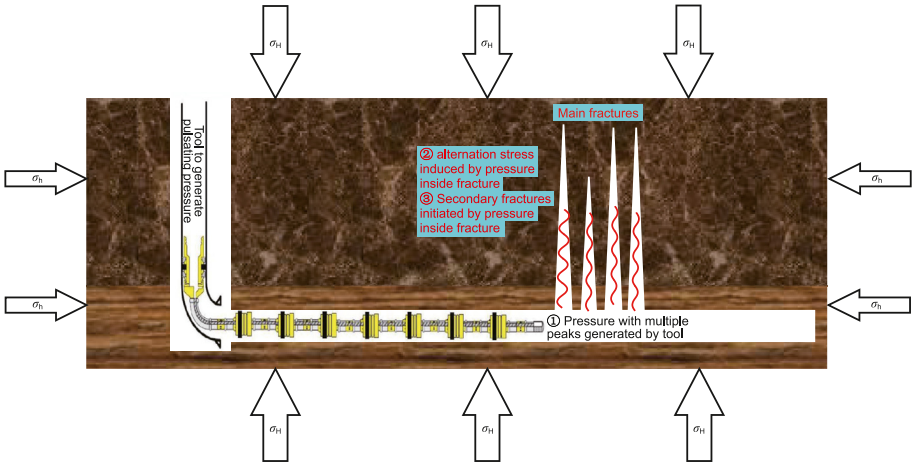

Fig. 1. Illustration of conceptual model of high-frequency pulsating hydraulic fracturing.

scheme (Zang et al., 2017b; Hou et al., 2021; Chang et al., 2022). The pulsating pressure propagates into main hydraulic fractures. If the frequency of pulsating pressure is over 10 Hz, the pressure distribution in main hydraulic fractures has multiple peak values (Hou et al., 2022a). The pressure inside fracture generated by common hydraulic fracturing methods is almost constant, which is different from the above pressure feature of the high-frequency PHF. The threshold of frequency to obtain the multiple peak values is over 10 Hz which is higher than the one of normal PHF method, therefore, this method is called as high-frequency PHF. The pressure inside fracture can trigger stress. If the stress meets rock damage criterion, the secondary fracture will be initiated.

The conceptual model for the above physical phenomenon is shown in Fig. 1. There are three physical processes: (1) the pulsating pressure (represented by the red wave line in Fig. 1) inside the main fractures is generated; (2) the rock deformation induced by the pulsating pressure and in-situ stress; (3) if the stress states of rocks around the main fracture is satisfied with rock damage criteria, the secondary fractures (represented by the yellow curves in Fig. 1) will be initiated. The tools to generate high-frequency pulsating pressure in reservoirs were proposed, such as self-excited pulsed jet device (Pang et al., 2022), hydraulic pulse oscillation tools (Shi et al., 2021).

2.2. Governing equations

In order to describe the above three physical phenomena, three governing equations are used in this study. The details of governing equations are shown in this section.

(1) Flow governing equation for pulsating pressure propagation

The fracturing fluid flow inside main hydraulic fractures during the PHF can be assumed as one-dimensional flow of single-phase liquid. In the PHF, the velocity of fluid satisfies the transient flow model, therefore, the momentum conservation law and mass conservation law of liquid are as follows (Fiorotto and Rinaldo, 1992; Hou et al., 2022b):

$$\frac{\partial v}{\partial t}+g\frac{\partial H}{\partial x}+\frac{f_D v|v|}{2D}=0 \tag{1}$$

$$\frac{a^2}{g}\frac{\partial v}{\partial x}+\frac{\partial H}{\partial t}=0 \tag{2}$$

where v represents the velocity of fluid, m/s; H represents the pressure head, m; There is a relationship between pressure head (H) and fluid pressure (p), $H = p/\rho g + z$, z represents the vertical location of fluid, m; g represents the gravity acceleration, m/s^2; ρ represents the fluid density, kg/m^3; a represents the propagation velocity of pressure wave in liquid, m/s, $a=(K/\rho)^{0.5}$; K represents elasticity modulus of fluid, GPa; f represents the Darcy-Weisbach friction factor; D is the equivalent diameter of the hydraulic fracture, which is calculated by: $D = 4 \times (A/S)$, m, A indicates the area of a fracture cross section, m^2, and S means the perimeter of the fracture cross section, m.

There are many models for Darcy-Weisbach friction factor. In this study, the Churchill equation (Churchill, 1997) is used:

$$f_D=8\left[\left(\frac{8}{Re}\right)^{12}+(c_A+c_B)^{-1.5}\right]^{\frac{1}{12}} \tag{3}$$

$$c_A=\left[-2.457\ln\left(\left(\frac{7}{Re}\right)^{0.9}+0.27\left(\frac{e}{D}\right)\right)\right]^{16} \tag{4}$$

$$c_B=\left(\frac{37530}{Re}\right)^{16} \tag{5}$$

$$Re=\frac{\rho VD}{\mu} \tag{6}$$

where Re represents the Reynolds number; e represents the roughness of the hydraulic fracture, m; μ is the fracturing fluid viscosity, Pa•s.

(2) Rock deformation equation

After the pulsating pressure is generated, it is applied at rocks and induces rock deformation. As shown in Fig. 1, the pulsating pressure is applied at main fracture surface so it can be an internal boundary condition for rock deformation. The governing equation for rock deformation is from the classical elasticity theory (Peng et al., 2021):

$$Gu_{i,kk}+\frac{G}{1-2\nu}u_{k,ki}=0 \tag{7}$$

where G represents the shear modulus of rock, $G=\frac{E}{2(1+2\nu)}$, E represents the Young's modulus of rock, GPa; ν represents Poisson's ratio, u represents the rock displacement, m, subscript i and k represent three directions.

When the stress induced by pulsating pressure satisfies with the rock damage criteria, the microscopic fractures are generated. According to rock damage theory (Zhu et al., 2018), the rock properties, such as Young's modulus, are changed when the rock damage occurs. Therefore, the damage variable is normal used to describe the alternation of Young's modulus induced by rock damage:

$$E_d=(1-d)E_0 \tag{8}$$

where E_d represents the updated Young's modulus with rock damage, GPa; E_0 represents the initial Young's modulus, GPa; d represents the damage variable. Substituting Eq. (8) into Eq. (7), the updated stress solutions after rock damage occurs can be obtained.

(3) Rock damage equation

According to the rock damage theory, the damage variable is defined as the ratio of broken rock to the whole representative volume element (Qu et al., 2019). Normally, it is assumed that the mechanical properties of the whole representative volume element are heterogeneous and the Weibull function is used to describe the heterogeneous distribution of mechanical properties (Zhu and Wei, 2011):

$$\varphi(z)=\frac{m}{z_0}\left(\frac{z}{z_0}\right)^{m-1}\exp\left[-\left(\frac{z}{z_0}\right)^m\right] \tag{9}$$

where $\varphi(z)$ is the probability density function of variable z; z_0 is the scale parameter of variable z; m is the homogeneity index of variable z and represents the dispersion degree of variable z. In this study, the strain in the whole representative element is assumed to be heterogeneous and the damage variable d equals to the

integration of Weibull distribution of strain:

$$\mathrm{d}(\varepsilon) = \int_0^{\varepsilon} \varphi(\varepsilon)\mathrm{d}\varepsilon \tag{10}$$

When the strain of the whole representative volume element is less than the threshold value ε_0, the representative volume element belongs to elastic stage. Otherwise, the rock damage occurs. Therefore, the damage variable model is as follows:

$$\mathrm{d}(\varepsilon) = \begin{cases} 0 \square\ \varepsilon \le \varepsilon_0 \\ 1 - \exp\left[-\left(\dfrac{\varepsilon - \varepsilon_0}{\varepsilon_0} \right)^m \right], \varepsilon > \varepsilon_0 \end{cases} \tag{11}$$

In this study, the maximum tensile criterion is used to judge whether the rock is broken so the threshold value of strain (ε_0):

$$\varepsilon_0 = \frac{\sigma_{\mathrm{ts}}}{E} \tag{12}$$

where σ_{ts} is the tensile strength of rock, MPa.

2.3. Numerical solving method

In order to numerically simulate the above three physical processes, three governing equations are used. The numerical solving method of these governing equations is complicated, the semi-explicit method is used to simplify the solving difficulty. The whole process is divided into several time steps. In each step, (1) the flow equations (Eq. (1)~(2)) that describes the pulsating pressure propagation behavior are first solved. (2) This solution is substituted into the rock deformation equation (Eq. (7)) to solve rock stress solution. (3) If the rock stress solution satisfies the damage criteria (Eq. (11)), the rock damage variable (Eq. (8)) would be updated. (4) The updated damage variable is then substituted into rock deformation equation to update the stress solution. If the updated stress solution also satisfies the damage criteria, the rock damage variable would be updated as well. (5) The fully coupled process terminates until the damage variable stop changing. One time step is finished and then the following time step continue to solve. The flow chart of semi-explicit method is shown in Fig. 2.

2.4. Model validation

(1) Validation of flow equation

In order to validate the flow equation as shown in Eq. (1)~(6), the experimental data obtained by Zhai et al. (2015) is compared with the numerical simulation data. The information of steel tube used in Zhai's experiment is shown in Fig. 3(a) and its length is 4.5 m and 6 measure points to measure pressure. The geometry and boundary condition used in the numerical simulation is shown in Fig. 3(b) and they are same with the ones in Zhai's experiment. The injection fluid is water and its density is 1000 kg/m^3 and viscosity is 3 mPa·s. The fluid is injected from the left side and the no flow boundary condition is set at the right end of pipe. The injection pressure is the pressure at Point 1 (P1) which is collected from the published paper of Zhai et al. (2015). The pressure at the Point 6 (P6) is used to validate the numerical result, as shown in Fig. 4. The average error between experimental and numerical results is only 1.01%. It indicates that the numerical model in this study is valid and can be used to analyze pressure applied at rock surface. The average error is calculated by Eq. (13):

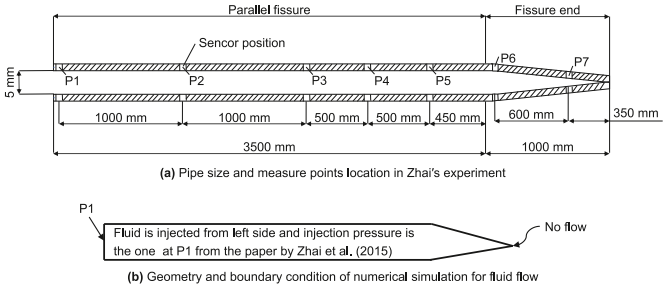

Fig. 3. Illustration of equipment in Zhai's experiment (**a**) and numerical geometry (**b**).

$$\delta = \frac{1}{n}\sum_{i=1}^{n} \frac{|V_{\mathrm{sim},i} - V_{\mathrm{count},i}|}{V_{\mathrm{count},i}} \times 100\% \tag{13}$$

where δ is the error, V_{sim} is the simulation data, V_{count} is the counterpart data which is experimental data or theoretical data, n is the number of data, i represents the data order.

(2) Validation of rock deformation equation

The stress induced by pulsating pressure that is described by Eq. (7) so the accuracy of this equation is important to analysis of rock damage induced by pulsating pressure. The geometry and boundary conditions in numerical simulation are shown in Fig. 5. The rock with a fracture is applied by two kinds of stress: maximum horizontal stress (σ_{H}) and minimum horizontal stress (σ_{h}). The homogeneous pressure (p) is applied at fracture surface. In this case, the conformal transformation method can calculate the stress around

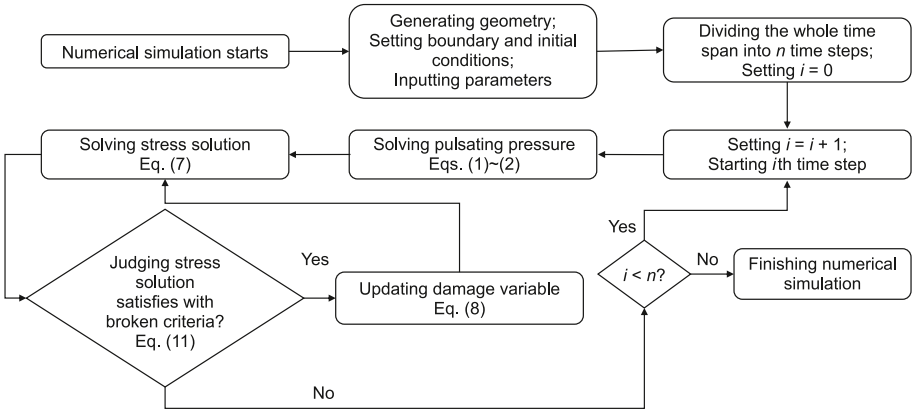

Fig. 2. Flow chart of semi-explicit method.

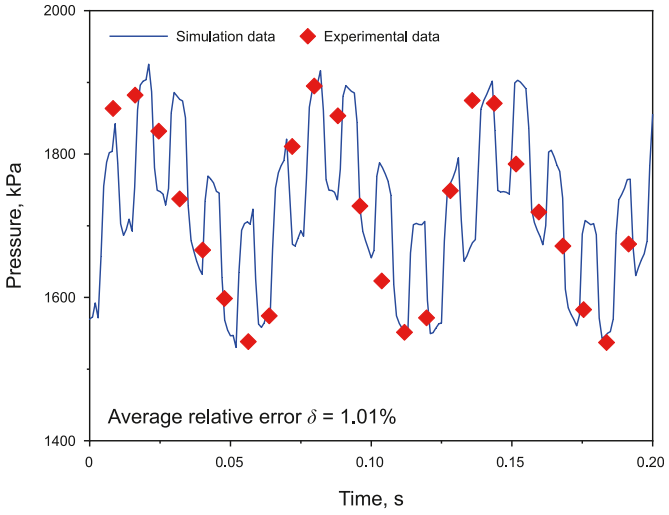

Fig. 4. Comparison between experimental and numerical results of fluid flow.

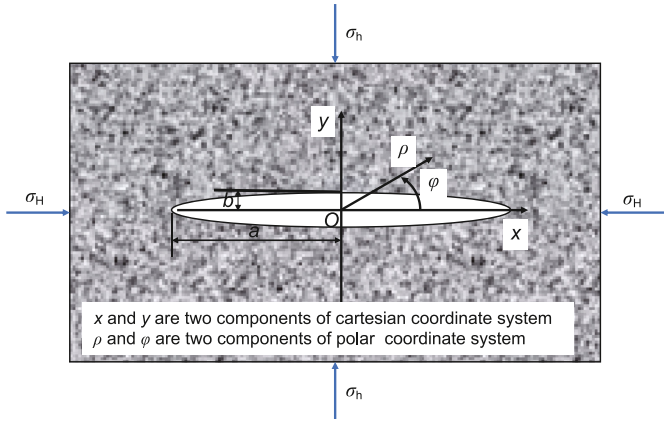

Fig. 5. Illustration of numerical model for validation of rock deformation equation.

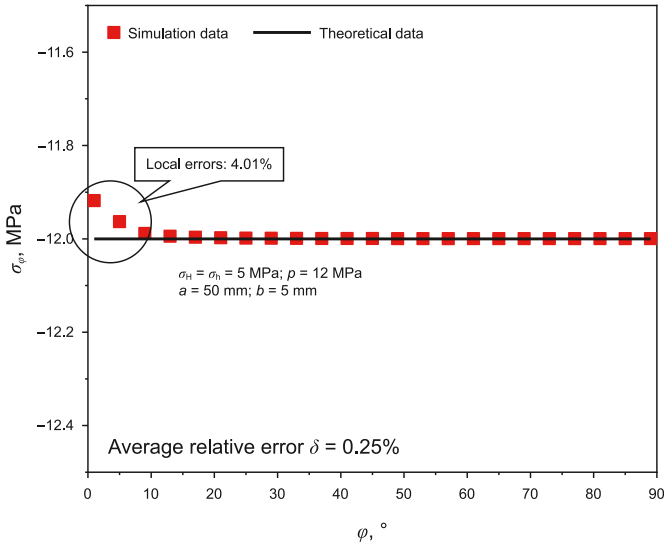

Fig. 6. Comparison between experimental and numerical results of rock deformation.

ellipse fracture (Peng et al., 2021) and the theoretical solution was proposed by Liu C. et al. (2022).

Fig. 6 shows the comparison between theoretical and numerical solutions for rock deformation equation. The parameters used in this case are also shown in Fig. 6. The average error between numerical solution and theoretical solution is also calculated by Eq. (13) and this average error is only 0.25%. It indicates that the governing equation for rock deformation is valid and can be used to analyze stress induced by pulsating pressure. However, the errors at low angle (0°~10°) are 4.01% and higher than ones at large angle. It is because that grids at low angle area cannot accurately represent its geometry and those grid inaccuracy bring higher errors at this area.

3. Mechanism of damage zone induced by pulsating pressure

3.1. Numerical model geometry and conditions

In this section, the characteristic of damage zone induced by pulsating pressure is investigated by numerical simulation. The 2D geometry model and boundary conditions are shown in Fig. 7. It is common that the hydraulic fracture propagation simulation is assumed as a 2D plane strain issue (Lei et al., 2021). With this assumption, it can decrease the solving difficulty and it is suitable when the fracture height is constant. The whole rectangle represents a reservoir, the ellipse in the center represents a half hydraulic fracture. The fluid is injected from the center of hydraulic fracture as shown a red point. The quarter of the whole geometry is selected due to the symmetry as shown in the right figure in Fig. 7. The right and bottom boundaries are applied by in-situ stress, σ_H and σ_h, respectively. The left and top right boundaries are applied by roller supports due to the symmetry of the whole geometry. The top left boundary is the hydraulic fracture surface and is applied by the pulsating pressure generated by fluid injection. The half-length of hydraulic fracture is 100 m and the maximum width of hydraulic fracture is 0.05 m. The quarter geometry size is 150 × 150 m. The pressure of the injection point is assumed as follows:

$$p_{in} = p_0 + p_{am}\sin(2\pi tf) \tag{14}$$

where p_0 is the average value of injection pressure, MPa; p_{am} is the amplitude value of injection pressure, MPa; f is the frequency of injection pressure, Hz; t is the time, s. The parameter values in the numerical simulation are shown in Table 1.

3.2. Characteristics of damage zone generated by pulsating pressure

After the common hydraulic fracturing is finished, the main hydraulic fracture is generated and then the high-frequency PHF is used to generate secondary fractures around the main hydraulic fracture. In this study, the rock damage is used to represent the initiation of secondary fractures generated by pulsating pressure.

The numerical solutions of rock damage zones around the main hydraulic fracture are shown in Fig. 8. There are three main characteristics of damage zones. (1) The damage zones are generated at different time. The time sequence of damage zones is Damage Zone 1, Damage Zone 2, Damage Zone 3 and Damage Zone 4. It indicates that enough time span is required to obtain more damage zones. (2) The required time span is not so big. The number of damage zones are fixed after a short time span. After 0.371 s, all the 4 damage zones are generated. After that, only the area of damage zones (represented by the black zones in Fig. 8) increases and the damage zone in the middle locations (zone 2 and zone 3 in this case) generate higher damage area than those in other locations as shown in Fig. 9. (3) The spatial distance between two nearby

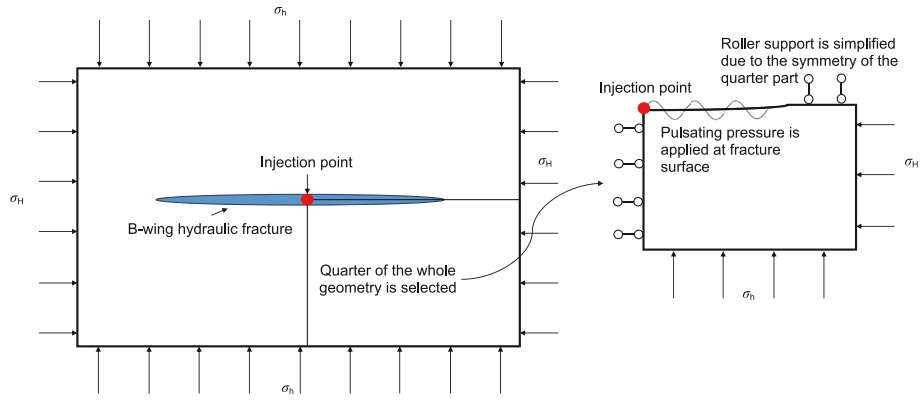

Fig. 7. Illustration of simulation model geometry and boundary conditions.

Table 1
Parameter values for numerical simulation (values cited from Zhu and Wei, 2011; Peng et al., 2021; Hou et al., 2022b).

Symbol	Value	Unit	Physical meaning
σ_H	25	MPa	Maximum horizontal stress
σ_h	15	MPa	Minimum horizontal stress
σ_{ts}	2	MPa	Tensile strength
σ_{pr}	80	MPa	Compression strength
p_0	10	MPa	Average value of injection pressure
p_{am}	8	MPa	Amplitude value of injection pressure
f	25	Hz	Frequency of injection pressure
ρ	2450	kg/m^3	Rock density
E_0	20	GPa	Young's modulus
υ	0.25		Poisson's ratio
μ	1	mPa·s	Fluid viscosity
m	2	–	homogeneity index

damage zones is about 28 m as shown in Fig. 8. It indicates that the zones around main hydraulic fracture can be fully stimulated by high-frequency PHF. The whole fracturing process includes two main modules: the conventional fracturing and the high-frequency PHF, therefore, the whole stimulation time equals to the sum of time for conventional fracturing and the time for the high-frequency PHF. In Figs. 8 and 9, the time value is only the time for the high-frequency PHF and it represents how much time the high-frequency pressure is applied to the rock.

In order to emphasize on the characteristics of secondary fracture initiation, based on the above numerical simulation setting, the pressure at injection point (red point in Fig. 7) is set as a constant value and this condition occurs in the common hydraulic fracturing (Goyal et al., 2020; Li M. et al., 2022). Normally, the pressure inside main fracture equals the sum of minimum horizontal stress and rock tensile strength. According to the parameters in Table 1, the pressure in this case is set as 22 MPa. The damage zone in this case is shown in Fig. 10. It is obvious that the common fracturing method only induces one damage zone at main fracture tip. It indicates the main fracture propagates. Its phenomenon is widely accepted by academic society (Lei et al., 2021). The difference of damage zone between Figs. 8 and 10 clearly illustrates the advantage of high-frequency PHF. This new hydraulic fracturing method can induce secondary fracture around the main fracture. It enhances the connectivity between main fractures and the whole fracture network volume, which can further enhance productivity.

3.3. Mechanism of damage zone generation

In this study, the tensile stress criterion is used to evaluate the damage zone generation. According to the geometry used in numerical simulation, the tensile stress around the main hydraulic fracture is stress in the x-direction (σ_x). The mechanism of damage zone generation can be analyzed by the σ_x distribution around the main hydraulic fracture, as shown in Fig. 11. When the σ_x is larger than the tensile strength (2 MPa in this case), the rock damage is generated.

During the PHF stimulation, the σ_x is always heterogeneous distribution along the main fracture. However, its distribution is time-dependent, therefore, all damage zones are not generated at same time and their generations occur from Zone 1 to Zone 4, as shown in Figs. 8 and 11. Fig. 12 shows the stress distribution induced by the common hydraulic fracturing stimulation (pressure inside main fracture is constant). The stress only has an obvious change at fracture tip due to the stress concentration and only the

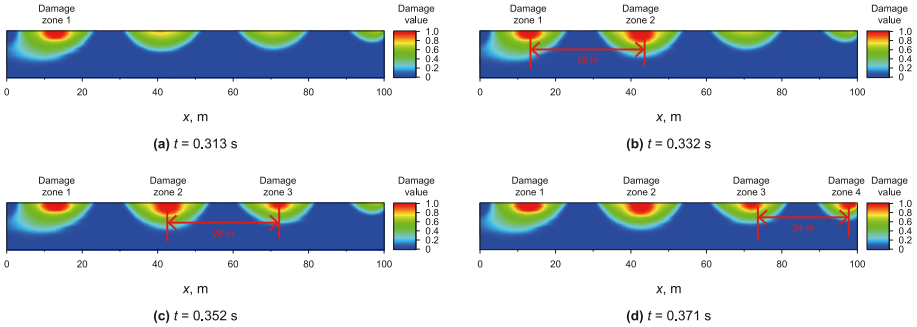

Fig. 8. Damage zone evolution during pulsating hydraulic fracturing stimulation (those time values are the time spans after pulsating pressure starts to be applied at the main fracture).

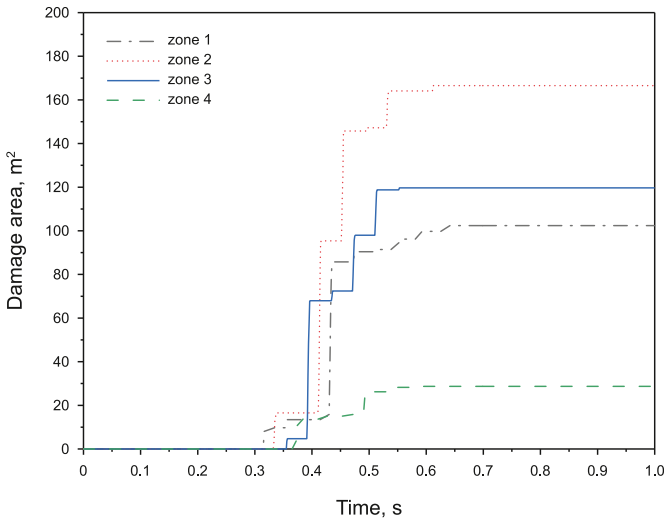

Fig. 9. Damage zone area evolution.

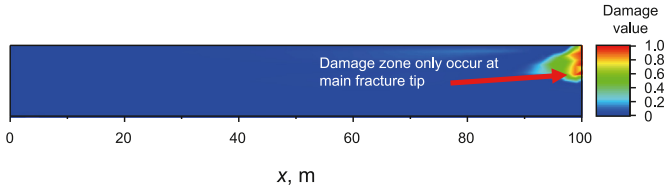

Fig. 10. Damage zone induced by common hydraulic fracturing stimulation (the pressure applied at rocks is constant and its value is 22 MPa which exceeds the minimum horizontal stress).

stress around fracture tip exceeds tensile strength. The difference of stress distribution generated by these two methods (as shown in Figs. 11 and 12) clearly illustrates the mechanism of damage zone generation induced by the PHF. The high-frequency PHF can induce tensile stress in the middle of main fracture and this tensile stress can exceed tensile strength. This spatial stress distribution results in the damage initiation.

In addition, the stress result from the above numerical simulation is further to compared with the theoretical solution to valid its accuracy. The stress solution induced by the heterogeneous distribution pressure inside fracture is extremely hard to be derived. In order to simplify the difficulty, the theoretical solution ignores the fracture existence and it is derived from the simple structure: the heterogeneous distribution pressure is applied at a semi-infinite solid as shown in Fig. 13(a). Based on the elasticity theory, the theoretical solution of σ_x in this case is:

$$\sigma_x(t) = -\frac{2}{\pi}\int_{h_0}^{h} \frac{p(\xi,t)x^3 \mathrm{d}\xi}{\left[x^2+(y-\xi)^2\right]^2} \tag{15}$$

where x, y are the coordinate components in two directions as shown in Fig. 13(a); ξ is the internal integration variable; h and h_0 are two ends of integration path; $p(\xi, t)$ is the dynamic pressure and can be obtained from the above simulation.

In order to compare with the theoretical solution, the almost same conditions are set for numerical simulation model but a fracture surface exists in numerical simulation, as shown in Fig. 13(b). The parameters used for theoretical and numerical solutions are shown in Table 1.

The comparison of stress distribution between theoretical and numerical solutions is shown in Fig. 14. It is obvious that stress distribution trends of theoretical and numerical solutions are same. If the homogeneous distribution pressure is applied at two models, stress distributions at fracture surface is also constant shown by the dashed lines in Fig. 14(a). Otherwise, if the heterogeneous distribution pressure is applied at two models, both theoretical and numerical models obtain the heterogeneous stress distributions at fracture surface shown by the solid lines in Fig. 14(a) and their alternation behaviors are the same but they have different values at some locations.

The gap between their values is induced by the difference of boundary conditions. The numerical simulation has a fracture structure but the theoretical model cannot have a fracture structure. The impact of boundary condition on stress solution can also be illustrated by the difference of solutions from the constant pressure as shown by the dashed lines in Fig. 14(a). In order to cancel out this impact, the difference of stress solutions from homogeneous pressure and heterogeneous pressure is shown in Fig. 14(b). In this case, the numerical solutions are almost the same with the theoretical solutions, and their average error is only 2.03% as shown in Fig. 14(b).

From the above analysis, the numerical solution has a same alternation trend from the theoretical solution; their values are almost the same if the impact of boundary condition is canceled out. Therefore, the numerical solutions shown in Figs. 8 and 11 are reliable. The heterogeneous stress distribution can really be induced by the heterogeneous distribution of pressure inside fracture during the PHF stimulation, and this heterogeneous stress distribution can really be induced tensile stress and damage zones around the main fracture. These solutions prove that high-frequency PHF method has a huge potential to initiate secondary fractures, enhance the connectivity between main fractures and increase fracture network volume.

4. Sensitivity study

In order to illustrate the factors affecting on damage zone generation, several sensitivity studies with the same geometry size in Fig. 7 are conducted in this section. Two groups of impact factors are investigated and they are geomechanical and stimulation factors.

4.1. Impact of geomechanical impact

In order to find out what kind of reservoir can be stimulated by high-frequency PHF, the impact of geomechanical properties on stress distribution is first investigated.

(1) Young's modulus

Normally, the Young's modulus range of rocks in reservoirs is 15~40 GPa so this range of Young's modulus is selected and other input parameters are the same with ones in Table 1. The numerical solution of stress around main fracture is shown in Fig. 15. It is clear that Young's modulus almost has no obvious impact of stress distribution. It is consistent with theoretical solution as shown in Eq. (15). The stress solution has no relationship with Young's modulus and it relates to pressure, boundary condition and fracture geometry size.

(2) in-situ stress

The hydraulic fracture propagation is importantly affected by the in-situ stress, especially the difference between two horizontal stresses. In this section, the range of stress difference is set as

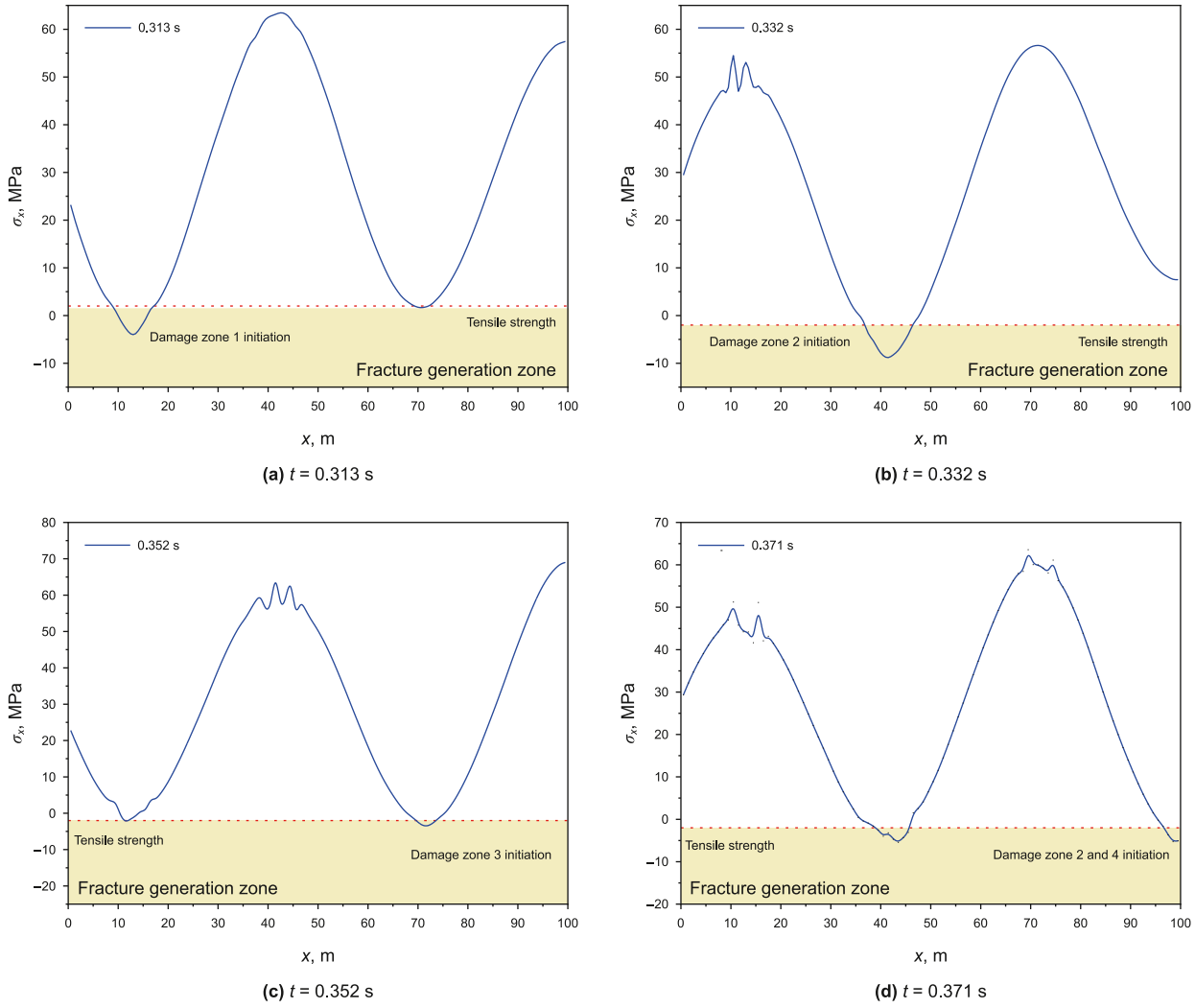

Fig. 11. Stress distribution evolution during pulsating hydraulic fracturing stimulation.

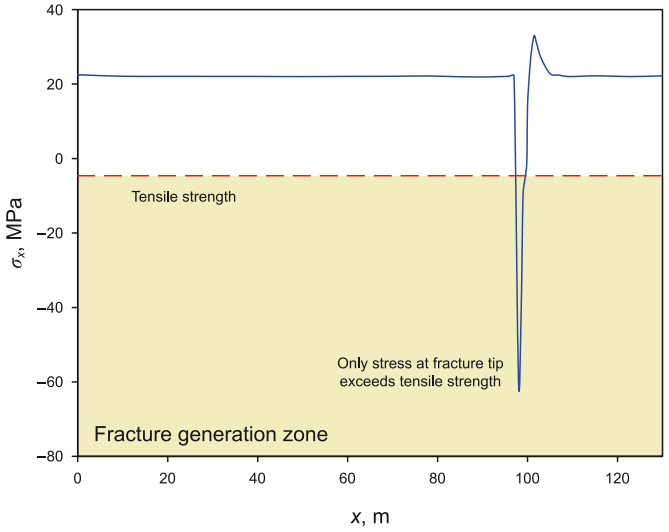

Fig. 12. Stress distribution induced by common hydraulic fracturing stimulation (the pressure applied at rocks is constant and its value is 22 MPa which exceeds the minimum horizontal stress.).

7–13 MPa and two groups are conducted, respectively: in one group, the maximum horizontal stress remains the same and only minimum stress changes; in the other group, the minimum horizontal stress remains the same and only maximum stress changes.

The stress solution is shown in Fig. 16. If the minimum stress changes, the tensile stress values alternate sharply but the compressive stress values are almost same, as shown in Fig. 16(a). If the maximum stress changes, all the stress values along the fracture surface alternate and the maximum tensile stress increases with stress difference, as shown in Fig. 16(b). The alternation of minimum stress plays a more important role on stress alternation than that of maximum stress. This phenomenon indicates that the minimum horizontal stress has more important impact on stress than that of the minimum one.

(3) Tensile strength

In this study, the rock damage is analyzed by maximum stress criterion as shown in Eqs. (11) and (12), therefore, the tensile strength is important for damage zone generation. The tensile strength range is set as 0.1–15 MPa and other parameters are shown in Table 1. The damage area evolutions for those cases are shown in Fig. 17. It is clear that the tensile strength decreases damage area. The damage area is extremely low and even fails to be

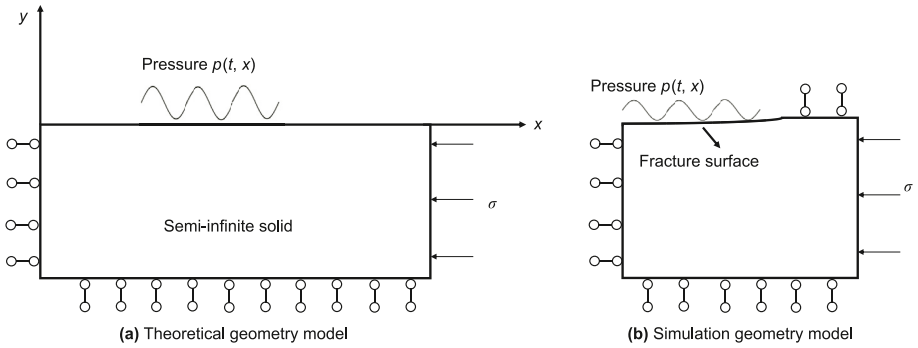

Fig. 13. Illustration about geometry models of theoretical and simulation.

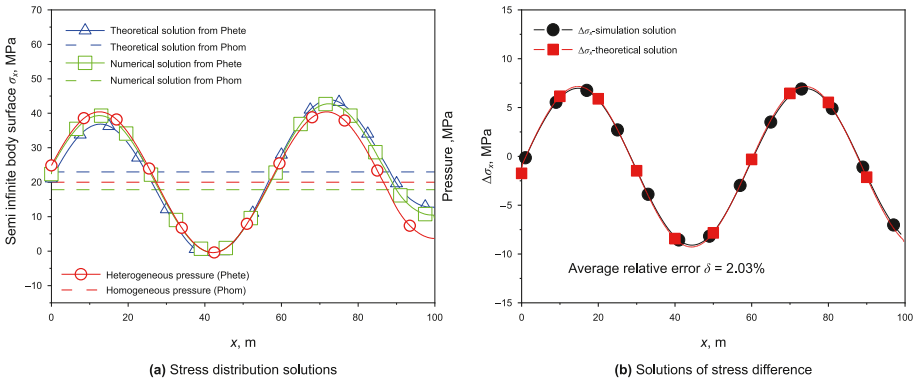

Fig. 14. Comparison of stress distribution between theoretical and numerical solutions.

generated after tensile strength exceeds 10 MPa. For the majority of reservoirs, the tensile strength is hard to exceed 10 MPa, therefore, this new hydraulic fracturing method can be widely applied.

The above solutions show that the damage zone generation difficulty magnitude has slight relationship with geomechanical factors. It indicates that the high-frequency PHF has a wide application potential for reservoirs with tough geomechanical properties.

4.2. Impact of stimulation factors

In the above simulations, the stimulation schedule remains the same. In order to find out how to improve stimulation efficiency, the impacts of stimulation factors on stress distribution are investigated in this section. The stimulation factors include average value of injection pressure (p_0), amplitude value of injection pressure (p_{am}) and frequency (f).

(1) Average value of injection pressure

Previous studies show that one of advantages of pulsating hydraulic fracturing is decreasing the injecting pressure (Hou et al., 2021), therefore, in this section, the average value of injection pressure (p_0) is set below the minimum horizontal stress. The other parameters are the same with ones in Table 1. The solutions of stress affected by average value of injection pressure (p_0) is shown in Fig. 18.

The impact of average value of injection pressure has a significant impact on stress distribution. The PHF can generate a dynamic pressure wave (Hou et al., 2022b) and its pressure is mainly dependent on superposition of several pressure waves. The pressure applied at fracture surface is heterogeneous, as shown in Fig. 18(b). The pressure applied at the location of wave peak is larger than the one at the location of wave trough. According the classical elasticity theory, the tensile stress can be generated by this kind of pressure distribution. If the p_0 is small, the pressure at wave trough is low and even a negative pressure value can be generated, as shown in Fig. 18(b). In this case, the tensile stress at wave trough is easily generated, as shown in Fig. 18(a). Therefore, the average value of injection pressure (p_0) has a significant impact of stress distribution.

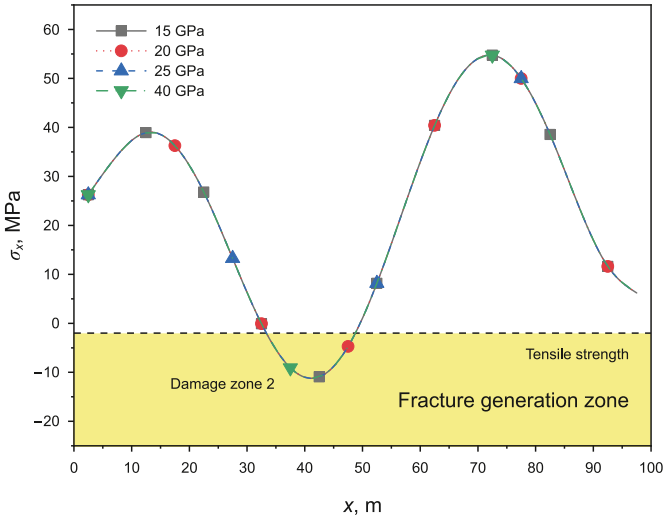

Fig. 15. The impact of Young's modulus on stress distribution.

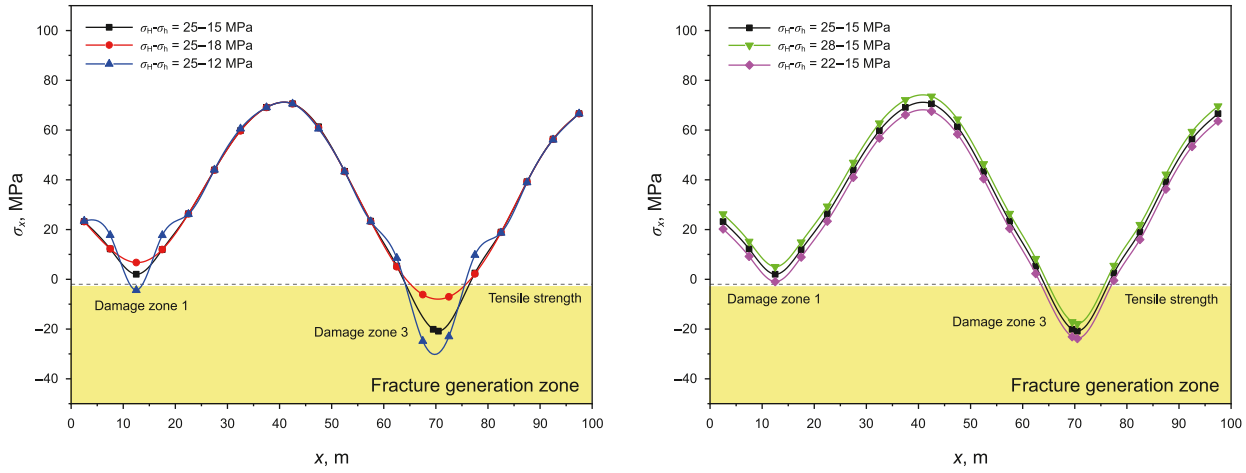

(a) Alternation of minimum horizontal stress **(b)** Alternation of maximum horizontal stress

Fig. 16. The impact of in-situ stress difference on stress distribution.

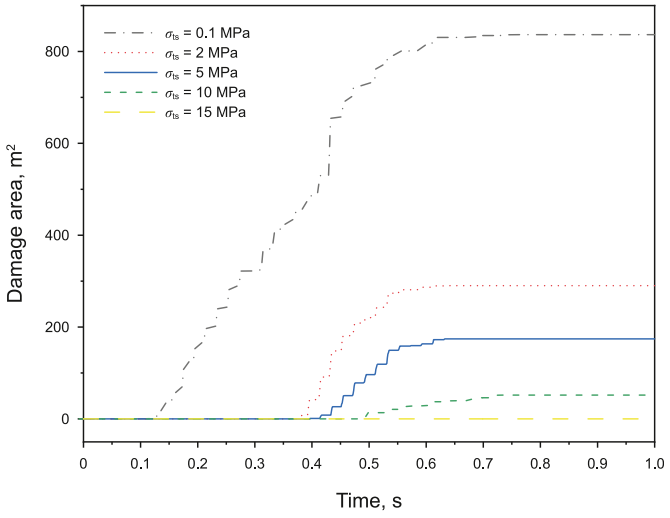

Fig. 17. Damage zone area evolution for rocks with different tensile strength values.

(2) Amplitude value of injection pressure

Amplitude value of injection pressure is one of important factors affecting pressure wave (Hou et al., 2022b), therefore, in this section, the amplitude value of injection pressure (p_{am}) is alternated but the other parameters are the same with ones in Table 1. The solutions of stress affected by amplitude value of injection pressure (p_{am}) is shown in Fig. 19.

The impact of amplitude value of injection pressure (p_{am}) has a significant impact on stress distribution. It is obvious that the maximum tensile stress increases with amplitude value of injection pressure (p_{am}). The alternation amplitude of maximum tensile stress is about 3 times higher than the amplitude value of injection pressure (p_{am}). The maximum tensile stress can be easily controlled by the amplitude value of injection pressure (p_{am}), therefore, the difficulty magnitude of damage zone generation can be decreased by increasing amplitude value of injection pressure (p_{am}).

(3) Frequency of injection pressure

Frequency of injection pressure is the other of important factors

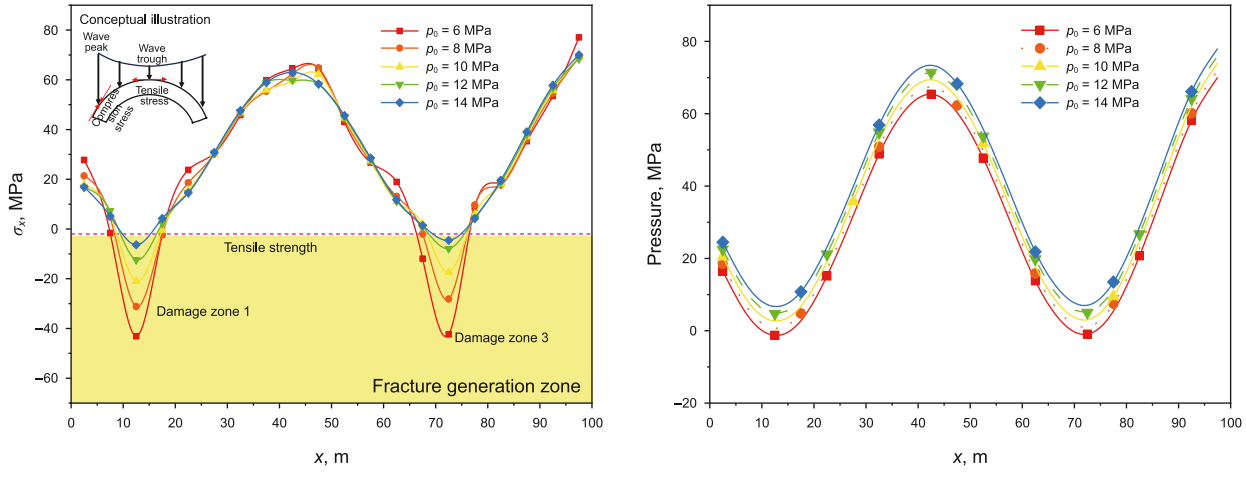

(a) Stress distribution **(b)** Pressure distribution

Fig. 18. The impact of average value of injection pressure on stress distribution.

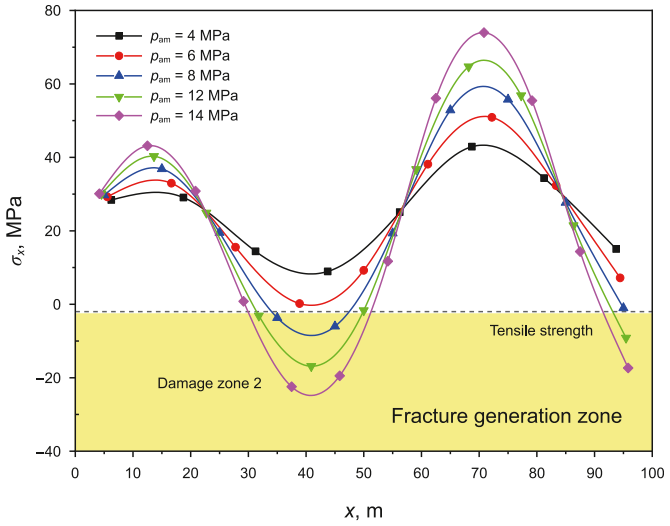

Fig. 19. The impact of amplitude value of injection pressure on stress distribution.

affecting pressure wave (Hou et al., 2022b), therefore, in this section, the frequency (f) is alternated but the other parameters are the same with ones in Table 1. The superposition of pressure wave occurs when the frequency exceeds 10 Hz for a 100 m-length fracture (Hou et al., 2022b), therefore, the frequency range is set from 15–50 Hz.

The spatial-temporal map of damage value evolution is shown in Fig. 20. It can be clearly seen that the frequency has an important role on damage zone evolution. Firstly, frequency has a close relationship with the damage zone number and the distance between two adjacent zones. Normally, the damage zone number increases with frequency, except for 30 Hz. There is only one damage zone when the frequency is 15 Hz, while, this number significantly increases to 4 when the frequency is 25 Hz, and it continuously increases to 7 when the frequency is 50 Hz. The distance between two adjacent damage zones decreases with frequency increases. This distance is 25 m when the frequency is 25 Hz and it decreases to 14 m when the frequency is 50 Hz. Secondly, frequency also affects maximum damage value. Although some frequency (f = 30 Hz, 50 Hz) obtain many damage zones, their maximum damage value is few. In this case, secondary fracture cannot be efficiently generated. In addition, Fig. 21 shows the stress distributions in the above cases. When the frequency values equal 25 and 40 Hz, the maximum tensile stress exists so the rock can be totally broken and the damage variable reaches at 1. In the other cases, there is no tensile stress so the rock cannot be totally broken and the damage variable is slight. It indicates that the frequency should be carefully selected and this principle is required more studies in the further.

(4) Importance magnitude of sensitive factors

If a factor affects fracture initiation significantly, the area of damage zone is large, therefore, the area value of damage zone can represent the importance of a factor. In order to compare the importance magnitudes between the above factors, the Pearson correlation coefficient method is used. This method can judge whether a factor has a linear relationship with the area value of damage zone. If the linear relationship is satisfied, the importance magnitudes of those factors can be compared by the slopes of linear relationship functions.

Table 2 shows analysis results of the above factors based on the Pearson correlation coefficient method. Based on the criterion of

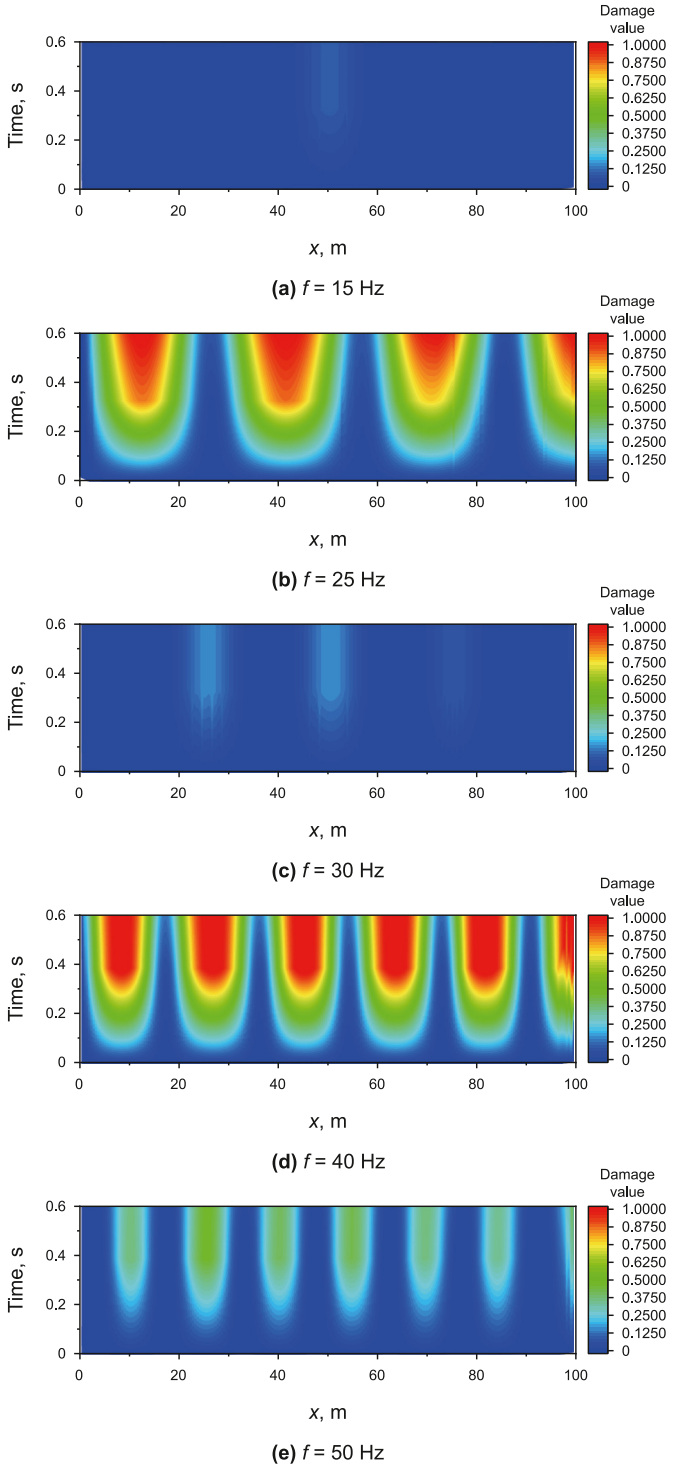

Fig. 20. Spatial-temporal map of damage value evolution for different frequency values.

this method, if the correlation coefficient ($|r|$) exceeds 0.8, the factor has a linear relationship with the area value of damage zone. Based on the results, the factors having a linear relationship includes: Young modulus (E_0), the maximum horizontal stress (σ_H), the minimum horizontal stress (σ_h), the tensile strength (σ_{st}), the average pressure (p_0) and the pressure amplitude (p_{am}). The importance magnitude can be judged by the slope value ($|k|$). The

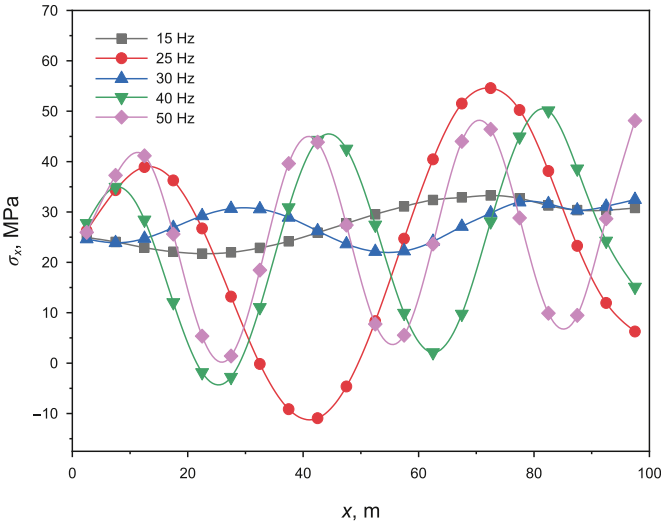

Fig. 21. The impact of frequency of injection pressure on stress distribution.

order of importance magnitude of these factors is: the pressure amplitude (p_{am}), the average pressure (p_0), the minimum horizontal stress (σ_h), the maximum horizontal stress (σ_H) and Young modulus (E_0).

From Fig. 20, it can be seen that the frequency has an important role in damage zone. However, the correlation coefficient ($|r|$) of frequency (f) is less than 0.8, so it does not have a linear relationship with area value of damage zone. The importance magnitude of frequency (f) cannot be directly compared with others. In order to simplify the comparison, the sensitivity index is proposed as shown in Eq. (16). It is the ratio of maximum alternation of damage zone area to the maximum alternation of factors. The ratio results of these factors are shown in Table 2. Based on these results, the importance magnitude of frequency is higher than the one of the maximum horizontal stress (σ_H). Based on these results, it is clear that the importance magnitudes of stimulation parameters (like p_0, p_{am} and f) is much greater than ones of geomechanical properties. Therefore, this new method can efficiently stimulate reservoirs.

$$\beta = \frac{y_{max} - y_{min}}{x_{max} - x_{min}} \tag{16}$$

where β represents sensitivity index of factor; y represents the area value of damage zone; x represents the value of a factor; the subscript 'max' represents the maximum value; the subscript 'min' represents the minimum value.

4.3. Application potential of high-frequency pulsating hydraulic fracturing

Based on the above analysis, the stimulation factors can significantly improve efficiency of damage zone generation, but the geomechanical characteristics in the above ones are not too tough. In this section, the potential of this new hydraulic fracturing method applied at some tough conditions is investigated.

(1) Reservoir with high maximum horizontal stress

When the maximum horizontal stress increases, the damage zone generation becomes difficulty, as shown in Fig. 16(b). However, the amplitude and frequency of injection pressure can decrease damage zone generation difficulty as shown in Figs. 19 and 20. In this section, the very tough condition of maximum horizontal stress is set and the optimized amplitude and frequency for this tough condition is found out. The maximum horizontal stress is set as 40 MPa and the stress difference between maximum and

Table 2
Comparison results of importance magnitude between different factors.

Factor symbol (unit)	Factor values	Damage zone area, m^2	$\|r\|$	$\|k\|$	β
E_0, GPa	15	286.39	0.92	4.13	0.21
	20	284.97			
	25	282.24			
	40	281.10			
σ_h, MPa	12	362.89	0.99	520.80	34.72
	15	284.91			
	18	154.57			
σ_H, MPa	22	302.43	1.00	153.28	6.13
	25	284.97			
	28	265.65			
σ_{st}, MPa	0.1	830.57	0.81	89.01	55.74
	2	284.97			
	5	168.34			
	10	45.91			
	15	0.00			
p_0, MPa	6	655.35	0.99	810.65	78.88
	8	490.13			
	10	284.97			
	12	130.91			
	14	24.31			
p_{am}, MPa	4	0.00	0.96	1262.70	149.96
	6	0.00			
	8	284.97			
	10	757.27			
	12	1199.70			
f, Hz	15	0.00	0.21	–	19.36
	25	284.97			
	30	0.00			
	40	677.72			
	50	0.00			

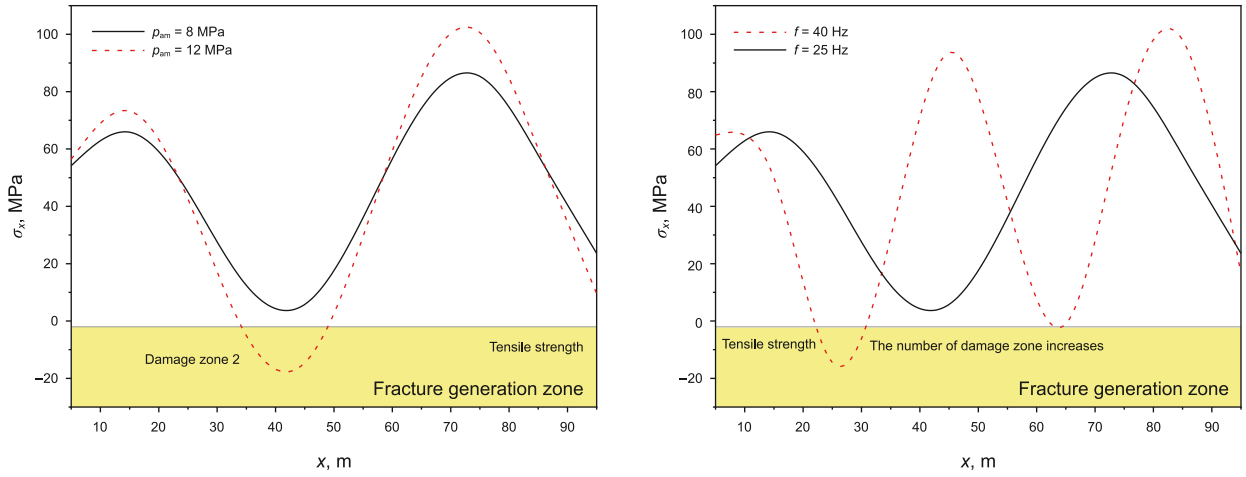

(a) Increasing amplitude p_{am} **(b)** Increasing frequency f

Fig. 22. Stress distribution in the condition of high maximum horizontal stress.

minimum stress is 20 MPa, other parameters are the same with ones in Table 1.

The stress distribution solution in this case is shown in Fig. 22. It is obvious that the maximum tensile stress does not exceed the tensile strength (shown as the black solid line), therefore, no damage zone is generated in these stimulation parameters shown in Table 1. Based on the above analysis in Section 4.2, there are two ways to improve stimulation efficiency. It is clearly seen from Fig. 22(a) that the maximum tensile stress exceeds the tensile strength if the pressure amplitude is 12 MPa. The other way to improve stimulation efficiency is to increase frequency. It is clearly seen from Fig. 22(b) that the maximum tensile stress exceeds the tensile strength if the frequency is 40 Hz and the damage zone number also increases in this case.

(2) Reservoir with high tensile strength

When the tensile strength exceeds 10 MPa, the damage generation becomes difficult as shown in Fig. 17. In this section, the very high tensile strength value (15 MPa) that rarely occurs in real reservoirs is set and the optimized amplitude and frequency for this tough condition is found out, other parameters are the same with ones in Table 1.

The stress distribution solution in this case is shown in Fig. 23. It is obvious that the damage zone can also be generated through optimizing pressure amplitude or frequency of injection pressure under this tough condition. Fig. 23(a) shows that the maximum tensile stress exceeds the tensile strength if the pressure amplitude is 12 MPa. Fig. 23(b) shows that the maximum tensile stress exceeds the tensile strength if the frequency is 40 Hz and the damage zone number also increases in this case.

The above solutions show that the damage zone generation difficulty magnitude has a significant relationship with stimulation factors. The damage generation difficulty can simply decrease by optimizing pressure amplitude or frequency of injection pressure. It indicates that the high-frequency PHF has a wide application potential for reservoirs even with tough geomechanical properties.

(3) Discussion about impacts of roughness and natural fractures

The surface of hydraulic fracture is usually rough and natural fractures are usually existed in reservoirs. The roughness of

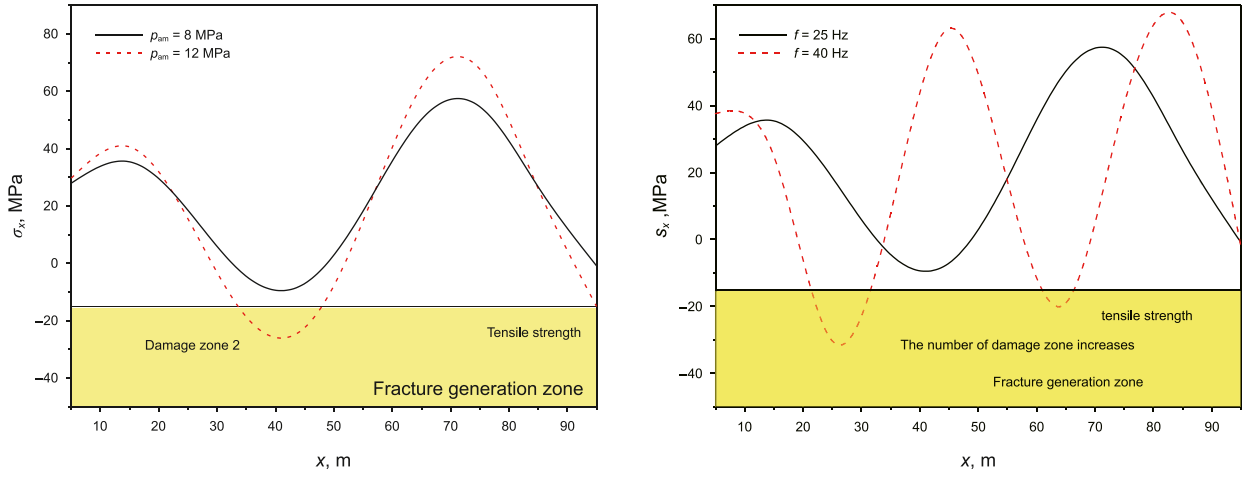

(a) Increasing amplitude p_{am} **(b)** Increasing frequency f

Fig. 23. Stress distribution in the condition of high tensile stress.

hydraulic fracture enhances the friction of fluid flow, and the natural fractures make the fluid leak from the HF into reservoir (Zhang et al., 2019; Wang et al., 2023). These phenomena normally make pressure inside fracture decrease (Hou et al., 2021; Cao and Sharma, 2022). If impacts of roughness and natural fractures are considered, the pressure inside fracture is lower than that without these impacts. The lower pressure inside fracture decreases the hydraulic fracture width and length (Cao and Sharma, 2022; Li N. et al., 2022). For the conventional hydraulic fracturing method, there are several models representing the impact of roughness on pressure. However, the fluid flow velocity for the high-frequency PHF significantly alternates, which is different from the one for the conventional hydraulic fracturing method. The impact of roughness on the pressure in this case is rarely investigated and there is no appropriate model to represent the impact of roughness. In this study, the accurate pressure alternation behavior induced by roughness and natural fractures cannot be predicted. According to the studies for the conventional hydraulic fracturing, the pressure inside fracture with these impacts can decrease. In this case, the generation difficulty of damage zone induced by the PHF increases and the application potential of the PHF can be restricted. The thorough investigation about impacts of roughness and natural fractures is required to be conducted in the future. In addition, the advantage of the PHF is to generate several damage zones around hydraulic fractures. The permeability of damage zone increases by several orders (Jiang et al., 2010; Zhu and Wei, 2011). The initial permeability range of shale reservoir and tight reservoir is from nanodarcy to micro-darcy. The production rate is low even after hydraulic fracturing. Several studies show that the oil and gas production of shale and tight reservoir will increase by about 163% if the permeability increase by 2 orders (Cui et al., 2018). Therefore, the high-frequency PHF is a promising method. The accurate production performance of the high-frequency PHF is required to be conducted in the future.

5. Conclusion

In order to investigate the mechanism of secondary fracture initiation induced by high-frequency PHF, a coupled numerical simulation model is proposed. Its validation is verified through experimental and theoretical solutions. Based on this model, the controlling factors are found out and its application potential for reservoirs is shown. The main conclusions are as follows.

(1) The coupled numerical simulation to investigate damage zone induced by the high-frequency PHF is valid. Through comparison with experimental and theoretical data, the average error of this simulation is less than 1%.
(1) The high-frequency PHF can induce many secondary fractures around the main fracture. This secondary fracture network is different from the one induced by the common hydraulic fracturing. It is because that the high-frequency PHF can induce tensile stress in several areas around the main fracture.
(3) The key geomechanical factors affecting secondary fracture initiation include the tensile strength and in-situ stress.
(4) The importance magnitudes of stimulation parameters are normally larger than ones of geomechanical properties. The average and amplitude of pressure can increase possibility of secondary fracture initiation. The frequency of pressure can increase number of secondary fractures. It indicates that this new method has a wide application potential.

CRediT authorship contribution statement

Yan Peng: Writing – original draft, Supervision, Methodology, Funding acquisition, Formal analysis, Data curation, Conceptualization. **Sheng-Jie Wei:** Writing – original draft, Formal analysis, Data curation. **Guang-Qing Zhang:** Supervision, Resources, Methodology. **Da-Wei Zhou:** Investigation, Data curation. **Chuang-Chao Xu:** Writing – review & editing, Validation.

Declaration of competing interest

The authors declare that they have no known competing financial interests or personal relationships that could have appeared to influence the work reported in this paper.

Acknowledgement

This work is supported by the National Natural Science Foundation of China (Grant No. 52004302), Science Foundation of China University of Petroleum, Beijing (No. 2462021YXZZ012), and the Strategic Cooperation Technology Projects of CNPC and CUPB (ZLZX2020-01).

References

Cao, M., Sharma, M., 2022. The impact of changes in natural fracture fluid pressure on the creation of fracture networks. J. Petrol. Sci. Eng. 216, 110783. https://doi.org/10.1016/j.petrol.2022.110783.
Chang, X., Xu, E., Guo, Y., et al., 2022. Experimental study of hydraulic fracture initiation and propagation in deep shale with different injection methods. J. Petrol. Sci. Eng. 216, 110834. https://doi.org/10.1016/j.petrol.2022.110834.
Cui, G., Liu, J., Wei, M., et al., 2018. Evolution of permeability during the process of shale gas extraction. J. Nat. Gas Sci. Eng. 49, 94–109. https://doi.org/10.1016/j.jngse.2017.10.018.
Churchill, S.W., 1997. Friction factor equation spans all fluid-flow regimes. Chem. Eng. 84, 2491–2492.
Ciezobka, J., Courtier, J., Wicker, J., 2018. Hydraulic Fracturing Test Site (HFTS)-Project Overview and Summary of Results. SPE/AAPG/SEG Unconventional Resources Technology Conference. 23–25 July, Houston, Texas, USA.
Diaz, M., Jung, S.G., Zhuang, L., et al., 2018. Hydraulic Mechanical and Seismic Observations During Hydraulic Fracturing by Cyclic Injection on Pocheon Granite. The ISRM International Symposium-10th Asian Rock Mechanics Symposium. Singapore.
Fiorotto, V., Rinaldo, A., 1992. Fluctuating uplift and lining design in spillway stilling basins. J. Hydraul. Eng. 118 (4), 578–596.
Goyal, S., Curtis, M.E., Sondergeld, C.H., et al., 2020. A Comparative Study of Monotonic and Cyclic Injection Hydraulic Fracturing in Saturated Tight Rocks Under Triaxial Stress. Proceedings of the 8th Unconventional Resources Technology Conference. Austin, Texas, USA, pp. 20–22. https://doi.org/10.15530/urtec-2020-2952.
Haimson, B.C., Cornet, F.H., 2003. ISRM suggested methods for rock stress estimation—Part 3: hydraulic fracturing (HF) and/or hydraulic testing of pre-existing fractures (HTPF). Int. J. Rock Mech. Min. Sci. 40 (2003), 1011–1020. https://doi:10.1016/j.ijrmms.2003.08.002.
He, P., Xiong, J., Lu, Z., et al., 2018. Study of pulse wave propagation and attenuation mechanism in shale reservoirs during pulse hydraulic fracturing. Arabian J. Sci. Eng. 43 (11), 6509–6522. https://doi.org/10.1007/s13369-018-3268-1.
He, X., Yang, J.J., Yang, B., et al., 2022. Experimental study of cavitating vortex rope and water column separation in a pump turbine. Phys. Fluids 34, 044101. https://doi.org/10.1063/5.0086509.
Hou, Y., Peng, Y., Chen, Z., et al., 2021. Investigation on the controlling factors of pressure wave propagation behavior induced by pulsating hydraulic fracturing. SPE J. 26 (5), 2716–2735. https://doi.org/10.2118/205384-PA.
Hou, Y., Peng, Y., Liu, Y., et al., 2022a. Influence of increasing mean stress on fatigue properties of shale during pulsating hydraulic fracturing. Energy Fuels 36, 14174–14186. https://doi.org/10.1021/acs.energyfuels.2c03064.
Hou, Y., Peng, Y., Chen, Z., et al., 2022b. Investigating heterogeneous distribution of fluid pressure in hydraulic fractures during pulsating hydraulic fracturing. J. Petrol. Sci. Eng. 209, 109823. https://doi.org/10.1016/j.petrol.2021.109823.
Ji, Y., Zhuang, L., Wu, W., et al., 2021. Cyclic water injection potentially mitigates seismic risks by promoting slow and stable slip of a natural fracture in granite. Rock Mech. Rock Eng. 54, 5389–5405. https://doi.org/10.1007/s00603-021-02438-7.

Jiang, T., Shao, J.F., Xu, W.Y., et al., 2010. Experimental investigation and micro-mechanical analysis of damage and permeability variation in brittle rocks. Int. J. Rock Mech. Min. Sci. 47 (5), 703–713. https://doi.org/10.1016/j.ijrmms.2010.05.003.

Jiang, Y., Xing, H., 2018. Theoretical research of pressure propagation in pulsating hydraulic fracturing for coal permeability enhancement. Int. J. Oil Gas Coal Technol. 17 (1), 91. https://doi.org/10.1504/IJOGCT.2018.10010324.

Jung, S., Diaz, M.B., Kim, K.Y., Hofmann, H., et al., 2021. Fatigue behavior of granite subjected to cyclic hydraulic fracturing and observations on pressure for fracture growth. Rock Mech. Rock Eng. 54, 5207–5220. https://doi.org/10.1007/s00603-021-02383-5.

Lei, Q., Doonechaly, N.G., Tsang, C.F., 2021. Modelling fluid injection-induced fracture activation, damage growth, seismicity occurrence and connectivity change in naturally fractured rocks. Int. J. Rock Mech. Min. Sci. 138, 104598. https://doi.org/10.1016/j.ijrmms.2020.104598.

Li, A., Zhu, J., Li, C., 2015. Further discussion on propagation model of fluctuating pressure in Crevice. J. Hydraul. Eng. 46 (5), 626–630. https://doi.org/10.13243/j.cnki.slxb.20140792 (in Chinese).

Li, M., Lv, W., Liu, J., et al., 2022a. Effect of perforation friction on 3D in-stage multiple fracture propagation: a numerical study. Eng. Fract. Mech. 267, 108415. https://doi.org/10.1016/j.engfracmech.2022.108415.

Li, N., Xie, H., Hu, J., et al., 2022b. A critical review of the experimental and theoretical research on cyclic hydraulic fracturing for geothermal reservoir stimulation. Geomech. Geophys. Geo-energ. Geo-resour. 8, 7. https://doi.org/10.1007/s40948-021-00309-7.

Liu, C., Zhang, D., Zhao, H., et al., 2022a. Experimental study on hydraulic fracturing properties of elliptical boreholes. Bull. Eng. Geol. Environ. 81, 18. https://doi.org/10.1007/s10064-021-02531-9.

Liu, P., 1994. Study on Erosion Mechanism of Rock Bed by Jetting Flow. PhD Dissertation. Tsinghua University, Beijing, China.

Liu, X., Li, B., Yue, Y., 2007. Transmission behavior of mud-pressure pulse along well bore. J. Hydrodyn. 19 (2), 236–240. https://doi.org/10.1016/S1001-6058(07)60054-7.

Liu, Y., Xu, T., Yuan, Y., et al., 2022b. A laboratory study on fracture initiation and propagation of granite under cyclic-injection hydraulic fracturing. J. Petrol. Sci. Eng. 212, 110278. https://doi.org/10.1016/j.petrol.2022.110278.

Ma, C., Jiang, Y., Xing, H., et al., 2017. Numerical modelling of fracturing effect stimulated by pulsating hydraulic fracturing in coal seam gas reservoir. J. Nat. Gas Sci. Eng. 46, 651–663. https://doi.org/10.1016/j.jngse.2017.08.016.

Oliveira, G., Franco, A., Negrao, C., et al., 2013. Modeling and validation of pressure propagation in drilling fluids pumped into a closed well. J. Petrol. Sci. Eng. 103, 61–71. https://doi.org/10.1016/j.petrol.2013.02.012.

Pang, H., Aibaibu, A., Xie, C., et al., 2022. Experiment and field application of a new self-excitedpulsed jet device. Acta Pet. Sin. 43 (2), 294–306. https://doi.org/10.7623/syxb202202011 (in Chinese).

Peng, Y., Liu, J., Zhang, G., et al., 2021. A pore geometry-based permeability model for tight rocks and new sight of impact of stress on permeability. J. Nat. Gas Sci. Eng. 91, 103958. https://doi.org/10.1016/j.jngse.2021.103958.

Qu, H., Peng, Y., Pan, Z., et al., 2019. A fully coupled simulation model for water spontaneous imbibition into brittle shale. J. Nat. Gas Sci. Eng. 66, 293–305. https://doi.org/10.1016/j.jngse.2019.03.028.

Rehbinder, G., 1980. A theory about cutting rock with a water jet. Rock Mech. Rock Eng. 12 (3–4), 247–257. https://doi.org/10.1007/BF01251028.

Shi, X., Huang, W., Gao, D., 2021. Mechanical behavior of drillstring with drag reduction oscillators and its effects on sliding drilling limits. Petrol. Sci. 18 (6), 1689–1697. https://doi.org/10.1016/j.petsci.2021.09.007.

Sławomir, H., 2018. Analytical Solution and numerical study on water hammer in a pipeline closed with an elastically attached valve. J. Sound Vib. 417, 245–259. https://doi.org/10.1016/j.jsv.2017.12.011.

Su, C., Camara, C., Kappus, B., et al., 2003. Cavitation luminescence in a water hammer: upscaling sonoluminescence. Phys. Fluids 15, 1457. https://doi.org/10.1063/1.1572493.

Sullivan, L., Grieser, B., 2017. Applying Enhanced Cyclic Diversion Process in Granite Wash Open Annulus Horizontal Completion. SPE Oklahoma City Oil and Gas Symposium Held in Oklahoma City. March, Oklahoma, USA 27–31.

Wang, F., Xu, J.X., Zhou, T., et al., 2023. Pump-stopping pressure drop model considering transient leak-off of fracture network. Petrol. Explor. Dev. 50 (2), 473–483. https://doi.org/10.1016/S1876-3804(23)60402-1.

Wang, W., Li, X., Lin, B., et al., 2015. Pulsating hydraulic fracturing technology in low permeability coal seams. Int. J. Min. Sci. Technol. 25 (4), 681–685. https://doi.org/10.1016/j.ijmst.2015.05.025.

Wu, J., Zhang, S., Cao, H., et al., 2020. Experimental investigation of crack dynamic evolution induced by pulsating hydraulic fracturing in coalbed methane reservoir. J. Nat. Gas Sci. Eng. 75, 103159. https://doi.org/10.1016/j.jngse.2020.103159.

Wu, X., Guo, Y., Chang, X., et al., 2023. Experimental study on cyclic hydraulic fracturing of tight sandstone under in-situ stress. Processes 11, 875. https://doi.org/10.3390/pr11030875.

Xu, D., Yuan, X., Wu, J., et al., 2019. Optimal design of cumulative shale gas hydraulic fracturing process based on rock fatigue damage theory. Integrated Ferroelectrics Int. J. 200 (1), 99–107. https://doi.org/10.1080/10584587.2019.1592625.

Xu, J., Zhai, C., Qin, L., 2017. Mechanism and application of pulse hydraulic fracturing in improving drainage of coalbed methane. J. Nat. Gas Sci. Eng. 40, 79–90. https://doi.org/10.1016/j.jngse.2017.02.012.

Xu, J., Zhai, C., Qin, L., et al., 2018. Pulse hydraulic fracturing technology and its application in coalbed methane extraction. Int. J. Oil Gas Coal Technol. 19 (1), 115–133. https://doi.org/10.1504/IJOGCT.2018.093962.

Zang, A., Yoon, J.S., Stephansson, O., et al., 2013. Fatigue hydraulic fracturing by cyclic reservoir treatment enhancespermeability and reduces induced seismicity. Geophys. J. Int. 195 (2), 1282–1287. https://doi.org/10.1093/gji/ggt301.

Zang, A., Stephansson, O., Zimmermann, G., 2017a. Keynote:fatigue hydraulic fracturing. Proc Eng 191, 1126–1134. https://doi.org/10.1016/j.proeng.2017.05.287.

Zang, A., Stephansson, O., Stenberg, L., Weber, M., et al., 2017b. Hydraulic fracture monitoring in hard rock at 410 m depth with an advanced fluid-injection protocol and extensive sensor array. Geophys. J. Int. 208, 790–813. https://doi:10.1093/gji/ggw430.

Zang, A., Zimmermann, G., Hofmann, H., et al., 2018. How to reduce fluid-injection-induced seismicity. Rock Mech. Rock Eng. 52 (2), 475–493. https://doi.org/10.1007/s00603-018-1467-4.

Zang, A., Zimmermann, G., Hofmann, H., et al., 2021. Relaxation damage control via fatiguehydraulic fracturing in granitic rock as inferred from laboratory-, mine-, and field-scale experiments. Sci. Rep. 11 (1), 1–17. https://doi.org/10.1038/s41598-021-86094-5.

Zhai, C., Yu, X., Xiang, X., et al., 2015. Experimental study of pulsating water pressure propagation in CBM reservoirs during pulse hydraulic fracturing. J. Nat. Gas Sci. Eng. 25, 15–22. https://doi.org/10.1016/j.jngse.2015.04.027.

Zhang, Q., Luo, S., Ma, H., et al., 2019. Simulation on the water flow affected by the shape and density of roughness elements in a single rough fracture. J. Hydrol 573, 456–468. https://doi.org/10.1016/j.jhydrol.2019.03.069.

Zhang, W., Shi, H., Li, G., et al., 2018. Fluid hammer analysis with unsteady flow friction model in coiled tubing drilling. J. Petrol. Sci. Eng. 167, 168–179. https://doi.org/10.1016/j.petrol.2018.03.088.

Zhao, Y., Liang, X., 1998. The propagation law of fluctuating pressure along the gap. J. Tianjin Univ. 3, 55–65 (in Chinese).

Zhi, Z., Zhi, Q., Jing, M., et al., 2017. Optimal design of shale gas hydraulic fracturing process based on fatigue damage theory. Flt Blk Oil Gas Field 24 (5), 705–708. https://doi.org/10.6056/dkyqt201705024.

Zhou, Z., Zhang, G., Dong, H., et al., 2017. Creating a network of hydraulic fractures by cyclic pumping. Int J Rock Mech Min 97, 52–63. https://doi.org/10.1016/j.ijrmms.2017.06.009.

Zhu, W., Liu, L., Liu, J., et al., 2018. Impact of gas adsorption-induced coal damage on the evolution of coal permeability. Int. J. Rock Mech. Min. Sci. 101, 89–97. https://doi.org/10.1016/j.ijrmms.2017.11.007.

Zhu, W.C., Wei, C.H., 2011. Numerical simulation on mining-induced water inrushes related to geologic structures using a damage-based hydromechanical model. Environ. Earth Sci. 62 (1), 43–54. https://doi.org/10.1007/s12665-010-0494-6.

Zhuang, L., Kim, K.Y., Jung, S.G., et al., 2019. Cyclic hydraulic fracturing of pocheon granite cores and its impact on breakdown pressure, acoustic emission amplitudes and injectivity. Int. J. Rock Mech. Min. Sci. 122, 104065. https://doi.org/10.1016/j.ijrmms.2019.104065.

Zhuang, L., Kim, K.Y., Jung, S.G., et al., 2020. Laboratory true triaxial hydraulic fracturing of granite under six fluid injection schemes and grain-scale fracture observations. Rock Mech. Rock Eng. 53, 4329–4344. https://doi.org/10.1007/s00603-020-02170-8.

Zimmermann, G., Zang, A., Stephansson, O., et al., 2019. Permeability enhancement and fracture development of hydraulic in situ experiments in the Äspö Hard Rock Laboratory, Sweden. Rock Mech. Rock Eng. 52, 495–515. https://doi.org/10.1007/s00603-018-1499-9.